Z. Phys. Chem. **222** (2008) 695–714 / **DOI** 10.1524/zpch.2008.5347

Electronic Spectra of Hydrogen-Bonded Self and Water Complexes of Indazole

By Erko Jalviste[1,*], Siarhei Dziarzhytski[2], and Friedrich Temps[2,**]

[1] Institute of Physics, University of Tartu, Riia 142, 51014 Tartu, Estonia
[2] Institut für Physikalische Chemie, Christian-Albrechts-Universität zu Kiel, Olshausenstr. 40, D-24098 Kiel, Germany

(Received October 22, 2007; accepted December 18, 2007)

Indazole / Hydrogen-Bonded Complexes / Molecular Beams / REMPI

Ultraviolet absorption bands of hydrogen-bonded dimers and trimers of indazole (Ia_2, Ia_3) and several indazole-water complexes ($Ia{\cdot}H_2O$, $Ia{\cdot}(H_2O)_2$, and $Ia_2{\cdot}H_2O$) have been identified in a He supersonic jet seeded with indazole vapor. Spectra were recorded using laser induced fluorescence (LIF) excitation, burn-probe type fluorescence-dip hole-burning, and one-color mass-resolved resonance enhanced two-photon ionization (R2PI) spectroscopies. Excitation laser power dependent changes in the spectra have been ascribed to optical saturation, dissociation by breaking of hydrogen bonds of a complex, and other fragmentation effects.

1. Introduction

The $S_1 \leftarrow S_0$ laser induced fluorescence (LIF) excitation spectrum of jet-cooled indazole (Ia) is characterized by a strong origin band at 290 nm and a relatively short vibronic progression assigned to vibrational modes of the indazole monomer [1]. The ground state vibrational frequencies of the molecule obtained from dispersed fluorescence measurements [1] are in good agreement with *ab initio* results [1] and with vapor-phase infrared absorption data [2]. A rotational analysis of the high-resolution spectrum of the $S_1 \leftarrow S_0$ origin band measured in a molecular beam [3] and in the vapor [4] confirmed that the observed electronic spectrum belongs to the 1H-Ia tautomer, which is more stable than the elusive 2H-Ia tautomer [5–7], since the same ground state rotational constants were obtained from the microwave spectrum [8] that unambiguously showed the 1H

* Corresponding author. E-mail: erko@fi.tartu.ee
** Corresponding author. E-mail: temps@phc.uni-kiel.de

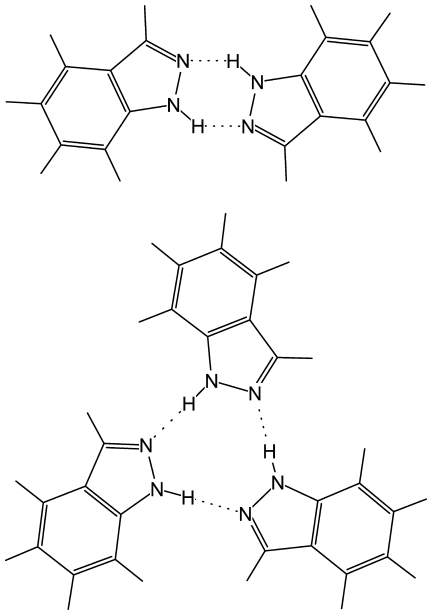

Fig. 1. Symmetric planar hydrogen-bonded structures of the indazole (≡benzopyrazole) dimer (Ia_2) and trimer (Ia_3) proposed by analogy with the *ab initio*–predicted structures of the dimer and trimer of pyrazole [10, 11].

structure. The adiabatic ionization energy of 1H-Ia, determined by mass analyzed threshold ionization spectroscopy, is 67 534 cm^{-1} [9].

Apart from the bands of the monomer, the LIF excitation spectrum of jet-cooled indazole showed several extra systems of weak bands red-shifted from the 1H-Ia origin [1]. These bands had been tentatively attributed to indazole-water clusters [1]. The present investigation was initiated in order to elucidate the nature of these bands in more detail. It will be shown that the dominating bands belong to the indazole dimer (Ia_2) and the indazole trimer (Ia_3), and that several indazole-water complexes ($Ia{\cdot}H_2O$, $Ia{\cdot}(H_2O)_2$, and $Ia_2{\cdot}H_2O$) are also present. Since the structurally prototypical five-membered heteroaromatic molecule pyrazole is known to form planar cyclic hydrogen-bonded self-association complexes in the gas phase [10, 11], one can imagine that indazole (≡benzopyrazole) can form analogous hydrogen-bonded cyclic dimers and trimers (see Fig. 1) that are stabilized in the cold supersonic jet. Such planar double bonded structures imply rather strong hydrogen bonding between the monomers, *ab initio* calculations for the pyrazole dimer for instance yielded a binding energy of ≈ 55 kJ/mol (4600 cm^{-1}, [11]). Furthermore, based on double hydrogen-bonded *ab initio* structures for pyrazole-water [12] and 3,5-dimethylpyrazole-acetic acid [10] 1:1 complexes, one may expect a similar structure for the lowest energy conformer of the $Ia{\cdot}H_2O$ complex as well.

Self-association governed by hydrogen bonding of pyrazole and a number of pyrazole derivatives with specific ring substituents has been extensively investigated under various conditions (crystal, liquid melt, solution, gas phase) using different (*e.g.*, X-ray scattering, NMR, IR, Raman) spectroscopic methods and *ab initio* calculations [10–11, 13–14]. Solid state NMR work demonstrated that several hydrogen-bonded structures can be prepared, depending on the pyrazole ring substitution [14–16]. For example, unsubstituted pyrazole has been found to form long chains, 3,5-diphenyl-4-bromopyrazole forms dimers, 3,5-dimethylpyrazole forms trimers, but 3,5-diphenylpyrazole forms tetramers. Infrared absorption measurements of pyrazole and 3,5-dimethylpyrazole vapor at different temperatures confirmed that both molecules exist in the gas phase in equilibrium mixtures of monomers, dimers, and trimers [10]. The three species were distinguished by their contributions to a broad (≈ 500 cm^{-1} wide) absorption feature in the NH/CH stretching region. Recently, Rice et al. [11] reported the infrared absorption spectrum of pyrazole complexes formed in a 60 cm wide pulsed slit jet. A band assigned to the pyrazole dimer gave a distinctive narrow peak at 3255 cm^{-1}. On enhanced cooling, multiple bands appeared in the trimer absorption region around 2900 cm^{-1} and, additionally, a quasi-continuous background absorption became much stronger, indicating the presence of even larger self-complexes and/or different conformers of the pyrazole trimer [11]. It would be difficult, however, to distinguish these pyrazole complexes by their electronic spectra, because the UV absorption spectrum of gas-phase pyrazole exhibits only a weak and unstructured onset at ≈ 5.5 [17].

Considering indazole, X-ray diffraction studies revealed that its crystal consists of infinite hydrogen-bonded chains, with the planes of neighboring molecules crossed [18]. Comparison of the IR spectrum in the NH/CH stretching region of indazole in the vapor phase [2] at ≈ 120 °C with the room temperature IR spectrum of polycrystalline indazole [2, 19] showed that in the solid phase the NH absorption feature is red-shifted by ≈ 300 cm^{-1} and about ten times broader. This can be explained by the presence of hydrogen-bonded structures in the solid. Direct spectroscopic measurements of electronic spectra of indazole dimers and trimers have not yet been reported as far we know. Fortunately, however, indazole in contrast to pyrazole exhibits a structured gas phase absorption spectrum and has a high fluorescence quantum yield. Moreover, since twice the value of the $S_1 \leftarrow S_0$ origin frequency (34 471.69 cm^{-1} [3]) exceeds the ionization energy (67 534 cm^{-1} [9]) of the molecule, one-color resonance enhanced two-photon ionization (R2PI) can be used for time-of-flight (TOF) mass spectrometry. These properties make ultraviolet jet spectroscopy, which has been successfully applied to a wide variety of hydrogen-bonded complexes [20–22], well suited to study possible complexes of indazole and determine their chemical compositions and structures.

In the present work, numerous UV absorption bands of indazole self and water complexes are distinguished and assigned to specific complexes by a combined analysis of a series of complementary spectra by different techniques,

namely LIF excitation spectra measured at different water concentrations in the carrier gas, fluorescence-dip UV-burn UV-probe hole-burning tests, one-color R2PI spectra detected at the mass of the selected species, and TOF mass spectra following excitation in selected absorption bands. It will be shown that optical saturation of the vibronic transitions (manifesting itself through a relative increase of the intensities of weaker bands at higher laser power) and fragmentation of the parent ions of the complexes (through breaking of hydrogen bonds) play significant roles and complicate the interpretation of the spectra.

2. Experimental section

LIF measurements were performed with an experimental setup as described in our previous work on the indazole monomer [1]. A pulsed He supersonic jet containing traces of indazole was formed by a heatable pulsed nozzle (General Valve #9) with a 0.8 mm pinhole. The indazole sample, used as supplied by Aldrich (98 %), was kept in a reservoir heated to 140 °C attached directly to the valve. Complexes with water were produced by flowing the He carrier gas through a small vessel with water or ice before entering the heated indazole reservoir. The water vessel was kept either at room temperature (20 °C) or it was cooled with ice (0 °C) or with an ice/salt mixture (−18 °C) to control the vapor pressure. LIF was excited by the unfocused beam (≈ 5 mm diameter) from a frequency-doubled pulsed dye laser (Spectra Physics PDL-3) pumped by a Nd:YAG laser (Continuum 661) operating at 20 Hz repetition rate. The emitted fluorescence was collected at right angles with respect to the jet axis and the laser beam by a photomultiplier tube (Hamamatsu R928) connected to a boxcar integrator (Stanford Research SR250) for signal gating and averaging. In most experiments, the excitation laser beam was aligned to cross the jet axis at a distance of about 15 mm downstream from the nozzle. However, since heavier clusters are known to be concentrated along the jet axis, while lighter species may be found in a wider cone, measurements were also conducted with the pump laser beam moved off-axis from the jet by about 6 mm to obtain size information on the complexes responsible for different bands. In order to minimize distortion of the relative band intensities in the excitation spectra by optical saturation, most of the LIF data were taken with the dye laser beam attenuated to ≈ 0.05 mJ/pulse by reflecting it from a fused silica glass plate, except for measurements of some partially saturated spectra (see below) which were recorded with up to ≈ 1 mJ/pulse.

R2PI spectra and mass spectra were measured using a linear time-of-flight (TOF) spectrometer with a 1.1 m long field-free drift tube. A 0.5 mm diameter skimmer (Beam Dynamics) about 15 mm downstream from a pulsed (10 Hz) heatable nozzle with a 0.5 mm pinhole separated the molecular beam source from the TOF chamber of the apparatus. The supersonic molecular beam of He seeded with indazole was generated as described above. For indazole-water

complexes, traces of H_2O vapor were introduced into the He carrier gas by temporarily connecting a room temperature vessel containing a few drops of H_2O to the He inlet tube. The vessel was then closed again and the measurements were performed shortly afterwards; the residual water vapor in the He sufficed to observe the complexes with indazole. The skimmed molecular beam entered the photoionization region through a 2 mm hole in the repeller electrode. The molecules and complexes were ionized by the unfocused beam (≈ 1.5 mm diameter) from a Nd:YAG pumped frequency doubled dye laser (Spectra Physics GCR-3 & Lambda Physics FL 3002) that crossed the molecular beam halfway between the repeller and an extractor plate. The electrode assembly, which is normally used for velocity map ion imaging [23], was converted to a three-electrode (repeller, extractor, ground) Wiley-McLaren setup [24] by covering the 20 mm diameter openings of the extractor and ground electrodes with nickel mesh. At the repeller-extractor and extractor-ground electrode distances of 12.5 mm and 19.5 mm, an optimal mass resolution (TOF peak width of 40 ns FWHM) was obtained with repeller and extractor voltages of 3000 V and 2760 V, respectively. The obtained ions were detected with a microchannel plate (Hamamatsu F4294–07) connected to a 350 MHz, 1 GSample/s digital oscilloscope (LeCroy LT264) for recording the mass spectra or to a boxcar integrator (Stanford Research SR250) with detection window set to 100 ns for measuring the mass-selected R2PI spectra. Typical ion arrival times with respect to the ionization laser pulse were 17.2 μs and 24.2 μs for the indazole monomer (Ia^+) and dimer (Ia_2^+), respectively. Mass spectra were obtained from the ion arrival time distributions, which were averaged over 500 laser shots, in the 50 μs time interval after the laser pulse, giving a mass range up to 1050 Dalton. The TOF scale was converted to the mass scale by the empirical relation $m(t) = (a + bt + ct^2)^2$, t being the measured arrival time in μs and m the corresponding mass in Dalton. The coefficients a, b, and c were determined from a fit to the arrival times and ion mass data of selected calibration peaks with known identity. In comparison with a two-parameter fit of the type $m(t) = (a + bt)^2$, the residual error of the mass peak positions in the covered mass range was reduced from about 0.7 Dalton to less than 0.2 Dalton. The R2PI measurements were performed with ≈ 0.1 mJ/pulse dye laser power, which provided a reasonable compromise between the increased noise level at too weak excitation and the onset of saturation and fragmentation effects in the spectra at too strong excitation.

UV-UV burn-probe fluorescence-dip hole-burning spectroscopy [25] was applied to identify bands belonging to the same species. Here, the observable dip caused by the burn pulse in the fluorescence excited by the probe pulse indicates that the burn and probe transitions start from the same ground state level of a complex that the strong burn pulse depletes, so that both transitions must belong to the same conformer of the same complex. For the hole-burning measurements, the Nd:YAG laser pumped two pulsed dye lasers (Spectra Physics PDL-3 and Lambda Physik FL3002) simultaneously. Both dye lasers were frequency doubled and had pulse energies of 1 mJ (burn) and 0.1 mJ (probe) measured just

before the vacuum chamber containing the He/indazole jet. The probe was delayed with respect to the burn by ≈ 45 ns (measured by detecting scattered laser light) by an optical delay line. Burn and probe were then spatially overlapped with the indazole containing molecular beam in a counterpropagating geometry. Instead of recording the entire hole-burning spectrum by scanning the burn wavelength with the probe wavelength set to a selected transition, we opted, in view of a relatively high noise level especially for bands of larger clusters, to individually check selected pairs of transitions for a possible common initial state. Towards these ends, the fluorescence signal induced by the probe was monitored in a 30 ns boxcar time gate, and the burn laser was sequentially blocked and unblocked every 30 s (600 laser shots) by a shutter. A decision whether the tested band pair belongs to the same species or not was then made depending on whether the resulting modulation of the probe signal intensity was at least as large or larger than the noise. For pairs of strong burn and weak probe transitions, where the tail of the exponentially decaying fluorescence induced by the burn pulse still gave a significant contribution to the fluorescence signal within the probe gate that partially obscured the hole-burning dip in the probe fluorescence, the burn-induced residual fluorescence was recorded separately with the probe beam blocked. The measured raw hole-burning traces were then corrected to determine the true hole-burning fluorescence dip.

3. Results and discussion

In the following, we describe (*i*) the LIF excitation spectra, (*ii*) the pump-probe hole-burning tests and (*iii*) the R2PI spectra of the indazole and indazole-water complexes. Progressions of bands in the spectra belonging to a separate complex were identified by tracking their intensity changes with changing experimental conditions (*e.g.*, added amount of H_2O) and by the hole-burning technique. Assignments to a particular indazole self or water complex were then made with the help of the R2PI spectra and the mass spectra. Additionally, (*iv*), we investigate mass spectra after excitation of selected bands and consider apparent laser fluence dependent fragmentation effects.

Identified separate band progressions are denoted in the text below by capital letters, “A”, “B”, etc. For the sake of clarity, and for easier reference, however, they are also labeled in the depicted spectra from the beginning on by the respective formulas, *i.e.*, $(Ia)_2$, $Ia{\cdot}H_2O$, etc., even though those assignments could be made with certainty only at the end.

3.1 LIF excitation spectra

LIF excitation spectra in the region from 289.9 nm to 293.6 nm measured at three different water vapor concentrations are shown in Fig. 2. As can be seen, the strongest band in all spectra is the origin band of the Ia monomer at λ

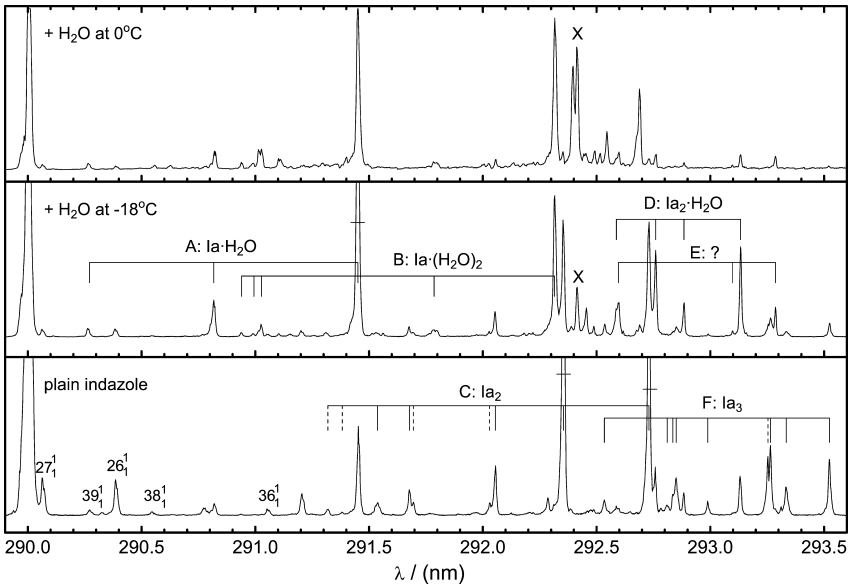

Fig. 2. LIF excitation spectra of indazole complexes at different water vapor concentrations in the carrier gas (indicated by the water vessel temperatures). The spectra were measured using an attenuated (≈ 0.05 mJ) unfocused pump laser beam (≈ 5 mm diameter) shifted 6 mm off-axis from the jet. Band progressions belonging to particular complexes according to the hole-burning tests and other criteria (see text) are marked by brackets with vertical lines and labeled with capital letters A–F. Progressions A–D and F were subsequently attributed to the specific complexes as indicated by their chemical formulas according to the mass-resolved R2PI spectra, progression E stayed unassigned. Hot bands of the Ia monomer are denoted by their respective mode numbers [1]. Horizontal bars mark the half-intensity values of bands extending out of the plot area. The intensity scales of the three panels are not related.

= 290.0 nm. The vibrational bands in the excitation spectrum of the monomer at shorter wavelengths have been firmly assigned [1]. All bands to the red of the monomer origin that are not hot bands were thus assigned to indazole complexes. Six groups of bands, which could be identified in this work, as detailed in the following, by their common behavior with changing experimental conditions, by hole-burning, and by R2PI spectroscopy are indicated by brackets, namely the progressions A–F. The band at 293.52 nm, which forms the origin of progression F, is the most strongly red-shifted assigned band in the spectra shown, although some very weak (more than ten times weaker) unassigned excitation bands were found even further to the red. Five bands in the bottom panel of Fig. 2 could be assigned to hot bands of the Ia monomer based on its known ground and excited state mode frequencies from our preceding work, they are indicated by their vibrational labels [1]. Some of the remaining weak unassigned bands may be additional hot bands of Ia monomer. Weak unaccounted other bands in the upper two panels measured with addition of H_2O presumably belong to larger

Table 1. Assigned vibronic bands in the LIF and R2PI spectra of the different indazole and indazole-water complexes in the order of increasing offsets of the band origins with respect to the origin of the Ia monomer. Transitions identified by hole-burning are marked by asterisks. $\nu_0^c - \nu_0^m$ is the frequency difference between the origin bands of the complex and the indazole monomer (ν_0^m = 34471.69 cm^{-1}, λ_{air}^m = 290.008 nm), [11] $\nu^c - \nu_0^c$ is the excited state vibrational frequency of the complex.

progression	assignment	λ_{air} (nm)	intensity	$\nu^c - \nu_0^c$ (cm^{-1})	$\nu_0^c - \nu_0^m$ (cm^{-1})
A	Ia·H_2O	291.451*	s	0	−171
		290.817*	m	75	
		290.271*	w	139	
		290.115	vw	158	
B	Ia·$(H_2O)_2$	292.315	s	0	−272
		291.786	w	62	
		291.027	m	151	
		290.994	w	155	
		290.940	w	162	
C	Ia_2	292.730*	s	0	−321
		292.354*	s	44	
		292.055*	m	79	
		292.030	w	82	
		291.695	w	121	
		291.678*	m	123	
		291.537*	m	140	
		291.382	w	158	
		291.319	w	165	
D	Ia_2·H_2O	293.133*	m	0	−367
		292.884*	w	29	
		292.760*	m	43	
		292.587*	w	64	
E	?	293.287*	m	0	−385
		293.097*	w	22	
		292.596*	m	81	
F	Ia_3	293.524*	m	0	−413
		293.334*	w	22	
		293.265*	m	30	
		293.253	w	32	
		292.989*	vw	62	
		292.850*	w	78	
		292.835*	w	80	
		292.810*	vw	83	
		292.534*	vw	115	

Ia_m·$(H_2O)_n$ complexes. One single band, denoted by "X", became quite strong at high H_2O addition (top panel).

The observed peak wavelengths, vibrational energies relative to the origin bands of the respective complexes, shifts of the complex origins with respect to the indazole monomer origin, and assignments of the progressions are compiled in Table 1. As shown, each progression consists of an origin band and several vibronic transitions involving low frequency (from 22 cm^{-1} to 158 cm^{-1}) vibra-

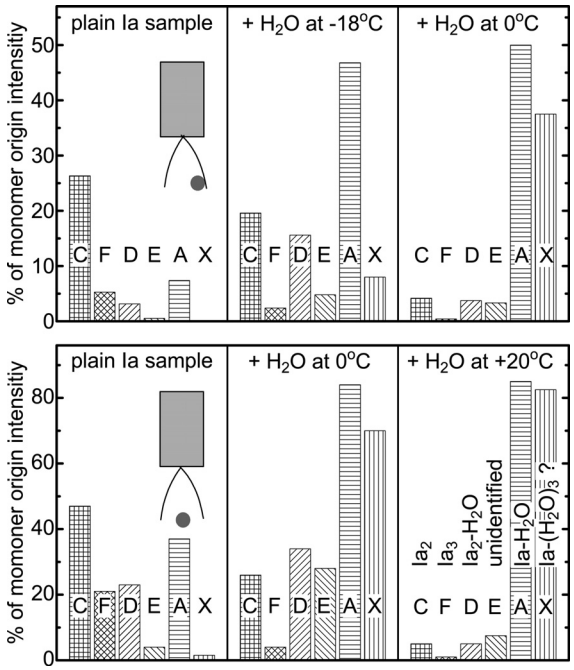

Fig. 3. Intensities of the origin bands of the observed complexes in the LIF excitation spectrum at different H_2O concentrations in the jet (see H_2O reservoir temperatures) in percent relative to the intensity of the indazole monomer origin band. From left to right, the data refer to the intensities of the origin bands (wavelengths and assignments in parentheses) of the progressions C (292.73 nm; Ia_2), F (293.52 nm; Ia_3), D (293.13 nm; $Ia_2{\cdot}H_2O$), E (293.29 nm; unidentified species), A (291.45 nm; $Ia{\cdot}H_2O$), and band X (292.41 nm; tentatively assigned to $Ia{\cdot}(H_2O)_3$). The assignments to particular complexes have been indicated for easier reference in the lower right panel. Upper row: pump laser beam off-axis; lower row: pump laser beam on-axis.

tions of the complexes in their excited electronic states. Obviously, the observed vibrations represent intermolecular motions between the Ia and/or H_2O monomer units in the complexes.

Fig. 3 shows the intensity of a representative vibronic band for each progression relative to the intensity of the monomer origin band under different experimental conditions. The height of each column in the different histograms shows the behavior of the respective progression. All data are for the origin bands of the progressions. The middle and right panels correspond to different partial pressures of H_2O, indicated by the temperature of the H_2O vessel, compared to the spectra obtained using the plain Ia sample on the left. As indicated by the small pictograms, the upper row refers to spectra measured with the pump beam crossing the jet off-axis and the lower row to spectra with the pump beam crossing the jet on-axis. The bands of the complexes in the on-axis case were up to four times stronger, showing that the ratio of the concentrations of complexes to

monomers is much smaller farther away from the jet axis. This tendency that heavier particles stay closer to the symmetry axis of a supersonic jet expansion is a well-known gas dynamic effect induced by collisions with carrier gas atoms. It can also be inferred from Fig. 3 that a higher H_2O concentration is needed in the on-axis than in the off-axis case (0 °C and 20 °C reservoir temperature instead of −18 °C and 0 °C) to induce similar intensity changes of the bands.

As can be seen from Fig. 3, the measured spectra of the plain Ia sample (without additional H_2O) are dominated by progression C. Progression F has slightly less than half the intensity of progression C in the on-axis case and is even weaker in the off-axis case, indicating that the complex giving rise to progression F is heavier than that responsible for progression C. Upon addition of H_2O, both C and F drop in intensity immediately (see also Fig. 2), which hints at indazole self complexes (*i.e.*, Ia_2 and Ia_3) rather than complexes with H_2O. As progressions C and F decrease with H_2O addition, progressions D, E and A as well as band "X" increase. Such behavior is consistent with formation of indazole-water complexes at the expense of self-complexes. Progression B, which was investigated less systematically and is not shown in Fig. 3, also increases (see Fig. 2). However, progressions D and E reach intensity maxima at some intermediate H_2O concentration, *i.e.*, their intensities first increase, but then decrease with higher H_2O. In contrast, progression A and band "X" increase along further with the H_2O concentration (right panels in Fig. 3), although some saturation seems to occur. As progression A is clearly the strongest under the off-axis conditions in the presence of H_2O, is has to originate from a relatively light complex, like $Ia{\cdot}H_2O$. This complex was visible as well in the molecular beam formed from the plain Ia sample in He owing to unavoidable residual traces of H_2O in the sample once the gas supply line was exposed to H_2O (see, for example, the origin band of progression A in Fig. 2 at λ = 291.45 nm). Only after very long baking and pumping of the supply line did the intensity of the intense origin band of progression A slowly decrease relative to the Ia monomer origin band. Thus, three major types of band progressions (C + F, D + E, and A + X) can be distinguished in the LIF excitation spectra based on the dependence of their intensities on the H_2O partial pressure.

Excitation with stronger pump pulses (1 mJ instead of 0.05 mJ/pulse) resulted in a relative enhancement of weak bands owing to saturation of the more intense transitions. This effect becomes apparent by comparing the unsaturated and saturated LIF excitation spectra given in the lower two panels of Fig. 4. Upon addition of water, the spectral density increased drastically. The excitation spectrum measured with 1 mJ laser pulses and high H_2O (20 °C reservoir temperature) has an almost continuous background, with an intensity of the background about half of that of the strongest bands (Fig. 4, top panel). The increasing congestions hints at the presence of larger $Ia_m{\cdot}(H_2O)_n$ complexes. These bigger complexes can exist in several conformers with different spectra, which eventually results in the observed continuous absorption. The absence of the continuum

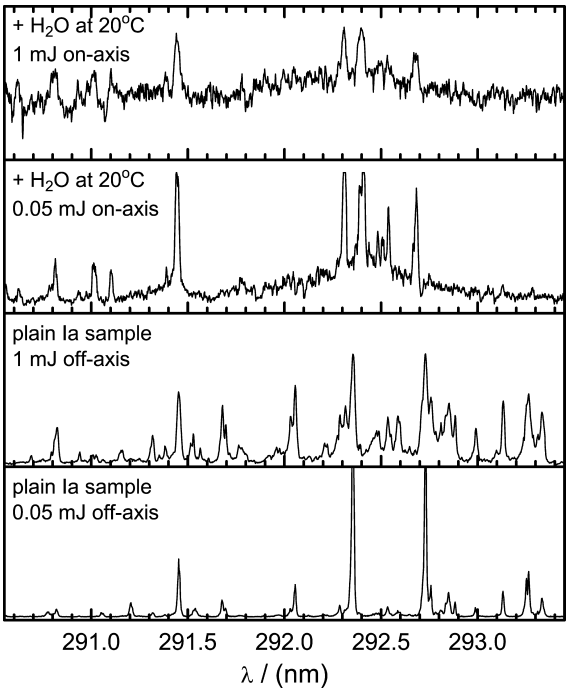

Fig. 4. Effect of optical saturation and water addition on the LIF excitation spectra under different experimental conditions. The zero of the vertical scales for all spectra corresponds to the zero-level of the signal intensity.

under weak excitation conditions is explained by smaller Franck-Condon factors of the bands of the larger complexes.

3.2 Hole-burning tests

Pump-probe fluorescence-dip hole-burning spectroscopy was used to distinguish separate progressions of absorption bands belonging to particular indazole complexes or different conformers. Since only a pair of transitions could be probed at a time, a routine test of 50 bands would have required probing of $50 \times 49/2 = 1225$ pairs. However, taking into account the information from the effect of increasing H_2O concentration on the LIF excitation spectra, only about 100 pairs of transitions had to be checked for a common ground state. For most band pairs, it was found to be advantageous to tune the burn laser to the stronger and the probe laser to the weaker transition of the pair, because the burn-induced depletion on weaker burn bands was too small to be detected. Only in cases, where a weak probe signal was obscured by strong fluorescence excited by the burn pulse was the burn laser tuned to the weaker transition. The observed maxi-

mal fluorescence depletion was about 30 %. It is noted as a caveat that a negative result of a hole-burning test does not necessarily suffice for the conclusion that the probed bands belong to different species. Other effects, like poor spatial overlap of the burn and probe beams, weakness of the burn transition, fluorescence excited by the burn beam, an accidental overlap with a neighboring band, or high noise on the probe transition can mask the fluorescence depletion signal.

The hole-burning tests allowed us to distinguish the progressions C and F as well as D and E from each other. The bands which were found to be related to each other have been marked by asterisks in Table 1. Additionally, some bands of progression C, which were too weak to produce observable hole-burning signals, were later identified from dispersed fluorescence spectra [26]. Furthermore, only three bands of progression A were identified by hole-burning, but the very weak fourth band at 209.12 nm appeared in an optically saturated R2PI spectrum (below). No hole-burning data were obtained for progression B; the bands listed in Table 1 were identified from the R2PI spectrum.

3.3 Mass selected R2PI spectra, assignment of progressions

Mass-selected R2PI spectra were measured in order to relate the identified band progressions to particular indazole complexes. Figs. 5 and 6 show the recorded spectra detected at the respective mass channels. An LIF excitation spectrum is depicted in the lowest panels of both figures for comparison.

Inspections of the spectra reveal the following:

1. The observation of progressions C and F in the R2PI spectra detected at the mass channels of Ia_2^+ and Ia_3^+, respectively, in Fig. 5 with the same band frequencies and similar band intensity distributions as in the respective LIF excitation spectra implies that they can be straightforwardly assigned to the indazole self complexes Ia_2 (progression C) and Ia_3 (progression F). On the same grounds, we can also assign a number of bands at the blue end of the Ia_2 and Ia_3 progressions, which were too weak to be identified by hole-burning. As was seen from Fig. 3, the dimer (C) and trimer (F) bands immediately decrease in intensity on addition H_2O to the jet, indicating formation of indazole-water complexes at the expense of the self-complexes.

   Interestingly, there is no evidence for trimer bands in the R2PI spectrum detected at the dimer mass. This indicates that fragmentation of Ia_3^+ yields Ia^+ rather than Ia_2^+ ions. Indeed, the R2PI spectrum detected at the Ia^+ mass also shows the features seen in the R2PI spectra detected at Ia_2^+ and Ia_3^+. Since the monomer cannot absorb in the region red from its origin, only fragmentation of trimers and dimers can give rise to these features in the Ia^+ R2PI spectrum. The somewhat higher intensities of the trimer bands compared to the dimer bands in the R2PI spectrum detected at the monomer mass reflects a higher dissociation yield for the trimer, probably owing to a lower binding energy of the trimer in its ionic state.
2. The four bands of progression D (λ = 293.13, 292.88, 292.76, and 292.58 nm) in the R2PI spectrum detected at the mass of Ia_2^+ in Fig. 5, which

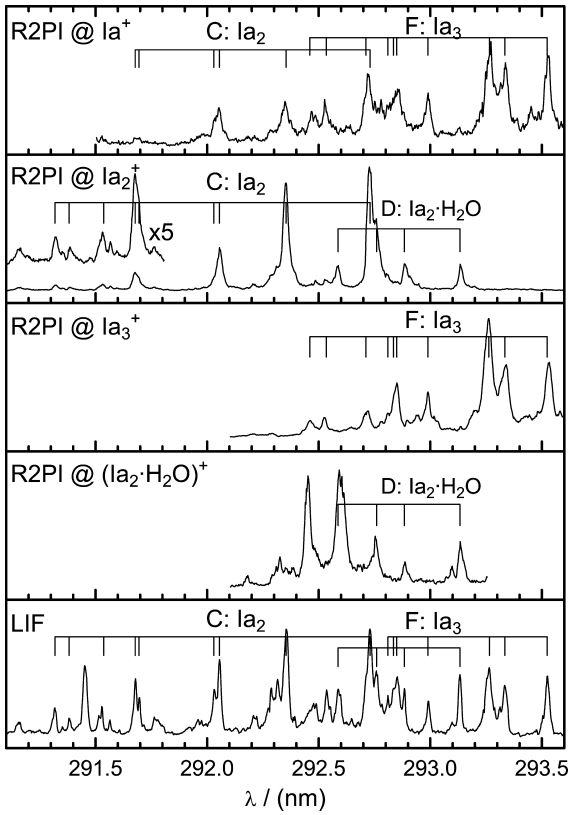

Fig. 5. Observed R2PI spectra detected at the mass channels of Ia, Ia_2, Ia_3, and $Ia_2{\cdot}H_2O$ and the (partially saturated, ≈ 1 mJ/pulse, off-axis pumped) LIF excitation spectrum from Fig. 4 for comparison. All R2PI spectra are measured with ≈ 0.1 mJ ionization laser pulses without water addition.

also appear in the LIF excitation spectrum but must belong to another species according to the hole-burning tests, can be assigned to $Ia_2{\cdot}H_2O$, because they appear also in the R2PI spectrum detected at the mass channel of that complex (fourth panel in Fig. 5). Three of them are red-shifted from the Ia_2 origin. The appearance of those bands in the R2PI spectrum detected at the dimer mass is explained by fragmentation of the $(Ia_2{\cdot}H_2O)^+$ complex to $Ia_2^+ + H_2O$ via hydrogen bond breaking. As noted from Fig. 3, the progression of $Ia_2 \cdot H_2O$ reaches its intensity maximum at some intermediate H_2O concentration, *i.e.*, the intensities first increase, but then decrease with higher H_2O.

3. In the R2PI spectrum detected at the $(Ia_2{\cdot}H_2O)^+$ mass (Fig. 5), the rather broad features at λ = 292.60 and 292.45 nm are much more intense than their counterparts in the LIF excitation spectrum, when the 293.13, 292.88 and

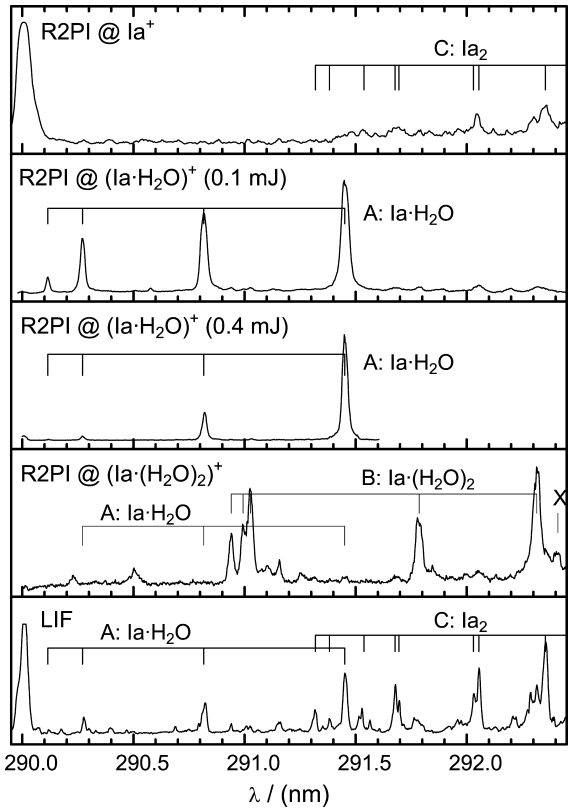

Fig. 6. Observed R2PI spectra detected at the mass channels of Ia, $Ia{\cdot}H_2O$, and $Ia{\cdot}(H_2O)_2$ and the (partially saturated, ≈ 1 mJ/pulse, off-axis pumped) LIF excitation spectrum from Fig. 4 for comparison. All R2PI spectra measured with ≈ 0.1 mJ ionization laser pulses (0.4 mJ in the third panel) without water addition, except for the $Ia{\cdot}(H_2O)_2$ R2PI spectrum measured with addition of water.

298.76 nm bands (cf. Table 1) are considered as typical for the $Ia_2{\cdot}H_2O$ complex. However, the 292.60 nm band in the R2PI spectrum consists of several overlapping features. Two of them appear to be distinguished in the LIF excitation spectrum in Fig. 2. The component at 292.596 nm was assigned to Progression D (*i.e.*, $Ia_2{\cdot}H_2O$) and the one at 292.587 nm to progression E. The 292.45 nm band and probably a third component of the 292.60 nm band, which are anomalously strong in the R2PI spectrum, may belong to a different $Ia_2{\cdot}H_2O$ conformer that is less easily fragmented. Alternatively, the bands at λ = 292.45 and 292.60 nm might come from fragmentation of $(Ia_2{\cdot}(H_2O)_2)^+$, although this is considered less plausible since they are suppressed with rising partial pressure of H_2O (Fig. 2).

4. Unfortunately, no R2PI or mass-spectral data were recorded to reveal the chemical identity of progression E so that its origin remains unknown.
5. As can be seen from Fig. 6, progression A was readily assigned to Ia·H_2O on the grounds that it clearly stands out in the R2PI spectra detected at that mass channel. As was noted from Fig. 3, the progression steadily increases along in intensity with rising H_2O concentration. The R2PI spectra shown in Fig. 6 for two different laser powers nicely demonstrate the effect of optical saturation on the band intensities and band widths. An additional band at λ = 290.12 nm appeared in the saturated spectrum, but is negligibly weak in the unsaturated case. The lack of corresponding features in the R2PI spectrum detected at the Ia^+ monomer mass indicates that $(Ia{\cdot}H_2O)^+$ exhibits little fragmentation compared to $(Ia_2{\cdot}H_2O)^+$ as well as Ia_2^+ and Ia_3^+. On the other hand, progression A of the Ia·H_2O complex was visible by LIF even in the plain Ia sample owing to hardly avoidable residual H_2O traces (see the Ia·H_2O origin band in Fig. 2 at λ = 291.45 nm.
6. The R2PI spectrum detected at the mass of $(Ia{\cdot}(H_2O)_2)^+$ is the one that led to a clear assignment of progression B to the Ia·$(H_2O)_2$ complex, which was only seen weakly in the LIF excitation spectra. This progression was not checked by hole-burning tests as its spectrum was to weak. The R2PI spectrum of the progression without addition of water to the jet was very weak and noisy. Addition of water, however, led to a moderately intense R2PI spectrum (Fig. 6), and thus to the assignment of progression B to the Ia·$(H_2O)_2$ complex.

   It is noteworthy that the band at λ = 292.315 nm, which can be identified as the Ia·$(H_2O)_2$ origin, is a strong band in the LIF excitation spectrum (cf. Fig. 2). However, the other prominent bands in the R2PI spectrum (291.79, 291.03, 290.99, and 290.94 nm) are very weak in the LIF spectrum. It is thus possible that these bands belong to a different Ia·$(H_2O)_2$ conformer.
7. The single band X at 292.41 nm, which was seen in the LIF excitation spectrum (Fig. 2), and which also appears in the R2PI spectrum detected at the $(Ia{\cdot}(H_2O)_2)^+$ mass, but is red shifted from the Ia·$(H_2O)_2$ origin, is tentatively assigned to the Ia·$(H_2O)_3$ complex. Presumably the third water is rater weakly bound so that the $(Ia{\cdot}(H_2O)_3)^+$ ion is expected to fragment easily to $(Ia{\cdot}(H_2O)_2)^+$ and H_2O. The remarkable increase of this band with rising H_2O partial pressure (see Fig. 3) is consistent with this assignment.

   Similar to the optical saturation effects in the LIF excitation spectra (see Fig. 4), the mass-selected R2PI spectra became more and more congested upon stronger excitation. Moreover, water addition to the He carrier gas gave rise to numerous new bands of larger indazole-water complexes, and their fragmentation added to the spectral congestion. Saturation and fragmentation is present to some extent in all spectra, but care was taken to minimize their effects by attenuating the ionization laser as far as possible by the signal-to-noise ratio.

3.4 Mass spectra and laser fluence dependent fragmentation

Further information was extracted from mass spectra recorded after exciting selected vibronic bands of the complexes using different laser powers (Fig. 7). Apart from supporting the above assignments of the band progressions to the respective species, the observed changes of the mass peak distributions with laser power, varied from ≈ 0.02 to ≈ 0.5 mJ/pulse, provide insight into the ionization and fragmentation dynamics.

1. As can be seen from the mass spectra after excitation of the vibronic bands assigned to Ia·H_2O, Ia·$(H_2O)_2$, Ia_2, and Ia_3 using weak laser pulses, the respective parent complex ions dominate the spectra. The exception, which will be discussed below, was Ia_2·H_2O. With higher laser powers, the mass peaks of Ia^+ can be seen to increase at the expense of the parent complexes, owing to increasing fragmentation by hydrogen bond breaking following intramolecular energy redistribution from the optically prepared highly excited state to intermolecular modes [22]. The fact that the parent ion dominates in the mass spectra at weak excitation suggests that, with the exception of Ia_2·H_2O, the one-photon excited singlet states and the two-photon excited cationic states of the complexes are not prone to fragmentation. The rapid increase of the fragmentation yields with higher laser powers suggests that significant fragmentation requires at least three photons.
2. Ia_3 seems to be relatively easily fragmented, since its mass peak increases only little before it declines with increasing laser power. In contrast, the $(Ia·H_2O)^+$ mass peak increases by a factor of six at ten times higher laser power. Also, the pattern of the mass spectrum of Ia·$(H_2O)_2$ seems to be retained even at high laser power. The appearance of an Ia_2^+ mass peak after excitation of the Ia·H_2O origin band hints at an accidental spectral overlap with a weak dimer band.
3. Excitation of the 293.13 nm band assigned to the Ia_2·H_2O origin gave only a weak mass peak of the parent complex ion compared with the apparent Ia_2^+ (and Ia_3^+) peaks. The presence of the trimer peak can be explained by an accidental spectral overlap; the R2PI spectrum of Ia_3 (see Fig. 5) indeed shows a weak feature at 293.13 nm. However, since the dimer origin is blue-shifted from the excited $Ia_2 \cdot H_2O$ band, an accidental overlap with a dimer band is not possible. Thus, the Ia_2^+ mass peak has to be attributed to fragmentation of Ia_2·H_2O. The considerable strength of the Ia_2^+ peak even with weak excitation pulses suggests that already the state of $(Ia_2·H_2O)^+$ that is reached with two photons is fragmenting. This hints at a significant difference between the potential surfaces of the neutrals and ions [22]. Water addition increased the $(Ia_2·H_2O)^+$ mass peak, but the Ia_2^+ mass peak always remained stronger than that of $(Ia_2·H_2O)^+$.
4. Excitation of the 292.60 nm band, which is one of the anomalously strong bands in the R2PI spectrum detected at the $(Ia_2·H_2O)^+$ mass, resulted in a mass spectrum similar to that of other $(Ia_2 \cdot H_2O)^+$ bands. However, the mass

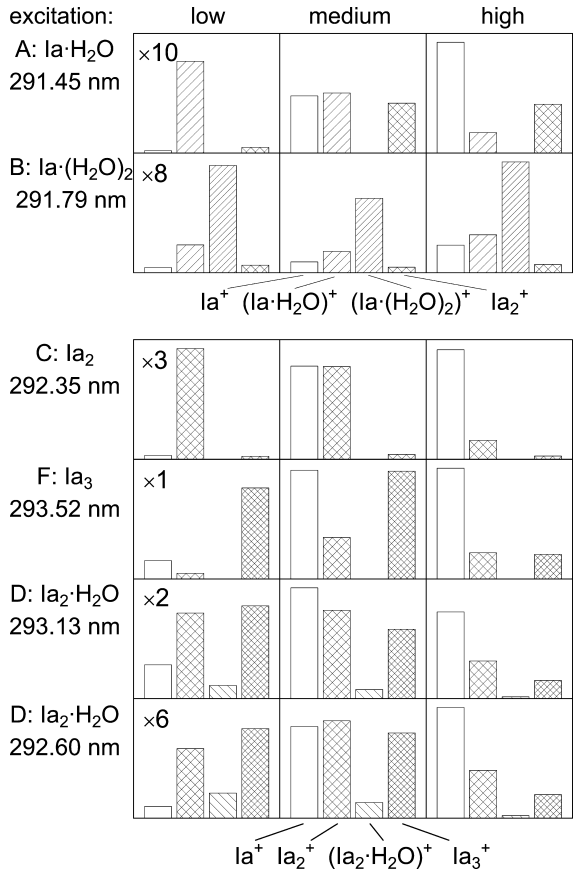

Fig. 7. Mass spectra recorded after exciting selected vibronic bands of the indazole complexes (see labels on the left) using different excitation laser powers (low: ≈ 0.03 mJ/pulse; medium: ≈ 0.2 mJ/pulse; high: ≈ 0.5 mJ/pulse). All data, except those for $Ia\cdot(H_2O)_2$ which were taken with addition of H_2O to the He carrier gas, were measured using plain Ia with an unfocused laser beam of ≈ 1.5 mm diameter. Note the different scaling factors for the left column.

peaks in that spectrum increased more strongly with increasing laser power (note the scaling factors in Fig. 7) than the mass peaks after excitation in the $Ia_2\cdot H_2O$ origin band. This corroborates the above-mentioned hypothesis that the strong bands at 292.60 nm and at 292.45 nm in the R2PI spectrum may belong to a less easily fragmented $Ia_2\cdot H_2O$ conformer.

5. Eventually, at higher mass ranges, series of weak, gradually decreasing mass peaks of indazole self-complexes up to Ia_9 appeared in all mass spectra. These large cluster peaks were almost independent of the excitation wavelength and laser power. Furthermore, addition of water to the He carrier gas

gave rise to long progressions of $Ia\cdot(H_2O)_x$and $Ia_2\cdot(H_2O)_y$ clusters with x, y ≤ 10 at the expense of the indazole self-complexes.

6. Last but not least, at the highest excitation powers, and especially when the excitation laser beam was focused into the indazole jet, ions with smaller masses than Ia^+ appeared owing to fragmentation of the Ia unit. Besides mass peaks of $C_nH_m^+$ (with n ≤ 6 and m ≤ 7), fragment peaks appeared at 89 to 92 Dalton. A prominent peak at 91 Dalton presumably results from loss of HCN (27 Dalton) from an indazole molecule (118 Dalton). We note that similar fragmentation patterns result from ionization of indazole by electron collisions [27]. Laser fluence dependent fragmentation of aromatic molecules accompanying multiphoton ionization by strong nanosecond laser pulses is a well known effect [28, 29] that is rationalized by sequential optical excitation, ionization, and fragmentation processes involving the generated ions (so-called ladder effect [29]).

4. Conclusions

Excitation spectra of a series of hydrogen-bonded self and water complexes of 1H-indazole have been investigated in a supersonic free jet expansion in the spectral region from λ = 289.9 nm to 293.6 nm, red from the origin band of the 1H-indazole monomer (λ = 290.0 nm), using LIF excitation, mass-resolved R2PI, and burn-probe hole-burning spectroscopies at different water concentrations in the He carrier gas and at different excitation laser powers. The origin bands and progressions of low-frequency excited state vibrations of the complexes Ia_2, Ia_3, $Ia\cdot H_2O$, $Ia_2\cdot H_2O$, and $Ia\cdot(H_2O)_2$ were unambiguously identified. All origin bands of the observed indazole complexes were found to be red-shifted compared to the origin of the Ia monomer. This indicates that the binding energies of the complexes in their excited states (S_1) are larger than the binding energies in their ground states (S_0). The observed vibronic bands, whose blue shifts from the respective origins range from 20 to 160 cm^{-1}, were ascribed to intermolecular vibrational motions in the complexes.

Double hydrogen-bonded planar structures were proposed for Ia_2 and Ia_3 by analogy with the known structures of the dimers and trimers of pyrazole. The observation of a series of equidistant weak mass peaks up to Ia_9 in the mass spectrum confirmed the presence of even larger indazole complexes. Upon addition of H_2O to the He carrier gas, the band intensities of indazole-water complexes in the spectra were observed to increase at the expense of the indazole self-complexes.

Higher excitation laser powers resulted in an increase of the relative intensities of weak bands in the LIF and in the R2PI spectra owing to optical saturation of the strong bands. At high H_2O concentration, the saturation effect led to a quasi-continuous background in the spectra, consistent with the presence of a large number of weakly absorbing higher complexes. Fragmentation of the ex-

cited parent complex ions via hydrogen bond breaking explains the observed Ia^+ monomer mass peaks with increasing excitation laser power. Fragmentation of the Ia^+ monomer unit was observed only after excitation by a strong, focused laser beam.

Overall, this study demonstrated the generation of a rich variety of self and water complexes of indazole with different chemical compositions and structures in a low-temperature supersonic jet. The tendency of indazole and water molecules to form double hydrogen bonds seems to play a major role. Having identified the different complexes, further information on the structures of the complexes can now be extracted from dispersed fluorescence spectra [26]. In addition, work is underway to identify intermolecular vibrational modes in the excited and in the ground states of the complexes using *ab initio* quantum chemical methods.

Acknowledgement

This work has been supported by the Deutsche Forschungsgemeinschaft and the Fonds der Chemischen Industrie and partially by the Estonian Science Foundation (Grants No. 6549 and 6550). E. J. is indebted to Dr. Attila Kuczmann for help with the initial experiments, Prof. Gerard Meijer for valuable advice, and the Alexander-von-Humboldt Foundation and Christian-Albrechts-University Kiel for the support of his visiting fellowship in Kiel.

References

1. E. Jalviste and F. Temps, J. Chem. Phys. **111** (1999) 3898.
2. E. Cané, R. Palmieri, R. Tarroni, and A. Trombetti, J. Chem. Soc. Faraday Trans. **89** (1993) 4005.
3. G. Berden, W. L. Meerts, and E. Jalviste, J. Chem. Phys. **103** (1995) 9596.
4. E. Cané, A. Trombetti, B. Velino, and W. Caminati, J. Mol. Spectrosc. **155** (1992) 307.
5. J. Catalán, J. L. G. de Paz, and J. Elguero, J. Chem. Soc. Perkin Trans. **2** (1996) 57 and ibid., (1996) 1027.
6. J. Catalán, J. C. del Valle, R. M. Claramunt, G. Boyer, J. Laynez, J. Gómez, P. Jiménez, F. Tomás, and J. Elguero, J. Phys. Chem. **98** (1994) 10606.
7. C. Ögretir and N. F. Kaypak, J. Mol. Struct. (Theochem) **583** (2002) 137.
8. B. Velino, E. Cané, A. Trombetti, G. Corbelli, F. Zerbetto, and W. Caminati, J. Mol. Spectrosc. **155** (1992) 1.
9. H. Su, M. Pradhan, and W. B. Tzeng, Chem. Phys. Lett. **411** (2005) 86.
10. J. P. Castaneda, G. S. Denisov, S. Y. Kucherov, V. M. Schreiber, and A. V. Shurukhina, J. Mol. Struct. **660** (2003) 25.
11. C. A. Rice, N. Borho, and M. A. Suhm, Z. Phys. Chem. **219** (2005) 379.
12. J. Limtrakul, Monatshefte für Chemie/Chemical Monthly **124** (1993) 259.
13. C. Foces-Foces, I. Alkorta, and J. Elguero, Acta Cryst. B **56** (2000) 1018.
14. O. Klein, F. Aguilar-Parrilla, J. M. Lopez, N. Jagerovic, J. Elguero, and H.-H. Limbach, J. Am. Chem. Soc. **126** (2004) 11718.
15. F. Aguilar-Parrilla, G. Scherer, H.-H. Limbach, M. C. Foces-Foces, F. H. Cano, J. A. S. Smith, C. Toiron, and J. Elguero, J. Am. Chem. Soc. **114** (1992) 9657.

16. J. L. G. de Paz, J. Elguero, C. Foces-Foces, A. L. Llamas-Saiz, F. Aguilar-Parrilla, O. Klein, and H.-H. Limbach, J. Chem. Soc. Perkin Trans. **2** (1997) 101.
17. I. C. Walker, M. H. Palmer, M.-J. Hubin-Franskin, and J. Delwiche, Chem. Phys. Lett. **367** (2003) 517.
18. P. A. Escande and J. Lapasset, Acta Cryst. B **30** (1974) 2009.
19. A. Bigotto and C. Zerbo, Spectrosc. Lett. **23** (1990) 65.
20. T. S. Zwier, Annu. Rev. Phys. Chem. **47** (1996) 205.
21. T. S. Zwier, J. Phys. Chem. A **105** (2001) 8827.
22. M. Mons, I. Dimicoli, and F. Piuzzi, Int. Rev. Phys. Chem. **21** (2002) 101.
23. J. Wei, A. Kuczmann, F. Renth, and F. Temps, Phys. Chem. Chem. Phys. **5** (2003) 315.
24. W. C. Wiley and I. H. McLaren, Rev. Sci. Instrum. **26** (1955) 1150.
25. R. J. Lipert and S. D. Colson, J. Phys. Chem. **93** (1989) 3894.
26. E. Jalviste and F. Temps, *unpublished results*.
27. NIST Chemistry WebBook (http://webbook.nist.gov).
28. C. Weickhardt, C. Grun, and J. Grotemeyer, Eur. J. Mass Spectrom. **4** (1998) 239.
29. U. Boesl, H. J. Neusser, and E. W. Schlag, Chem. Phys. Lett. **87** (1982) 1.